Fluid-membrane tethers: Minimal surfaces and elastic boundary layers

Thomas R. Powers,[1,*] Greg Huber,[2,†] and Raymond E. Goldstein[3,‡]

[1]*Division of Engineering, Brown University, Providence, Rhode Island 02912*
[2]*Department of Physics, University of Massachusetts at Boston, Boston, Massachusetts 02125*
[3]*Department of Physics and Program in Applied Mathematics, University of Arizona, Tucson, Arizona 85721*

Thin cylindrical tethers are common lipid bilayer membrane structures, arising in situations ranging from micromanipulation experiments on artificial vesicles to the dynamic structure of the Golgi apparatus. We study the shape and formation of a tether in terms of the classical soap-film problem, which is applied to the case of a membrane disk under tension subject to a point force. A tether forms from the elastic boundary layer near the point of application of the force, for sufficiently large displacement. Analytic results for various aspects of the membrane shape are given.

I. INTRODUCTION

Imagine a soap film connecting two nearby parallel rings that are slowly pulled apart. The film evolves through a series of catenoids until the ring separation reaches a critical value. Then the film breaks. Now imagine performing the same experiment with microscopic rings connected by a lipid bilayer membrane. In this paper, we will show that the membrane forms catenoidal shapes at small ring separations, but instead of breaking, the membrane forms a thin cylindrical tether for sufficiently large displacement.

A situation very much like this imaginary experiment arises in a host of real experiments on artificial vesicles, living cells, and organelle membranes such as that of the Golgi apparatus. Perhaps the most controlled tether experiment is that of Evans and Yeung, in which a tether forms when a quasispherical vesicle held at a fixed tension is made to adhere to a stationary bead, and then withdrawn [1]. There are many variations on this experimental theme [2–6], and such experiments have been used to measure a wide variety of membrane mechanical properties [7].

Tethers commonly form in less controlled situations as well. Simply pulling on a vesicle or cell with a sufficiently large point force leads to a membrane tether (Fig. 1). Tethers form when tubulin trapped inside a vesicle polymerizes to form microtubules [8]: as the microtubules grow, the initially spherical membrane at first distorts into an ellipsoidal shape, and then eventually forms a surface of revolution with a contour in the shape of the Greek letter "ϕ" [9–11]. Improvements in staining techniques have recently revealed dynamic tether networks in the Golgi apparatus of living cells [12]; similar model membrane networks have been studied *in vitro* and used as templates for making more durable networks [13].

The variety of conditions under which tethers occur shows that they are robust structures, insensitive to the details of applied forces and boundary conditions. Despite much theoretical, computational, and experimental attention, a simple intuitive picture for tether formation that exploits the insensitivity to geometric constraints (such as volume conservation) and emphasizes the role of the most essential control parameters has yet to emerge. It is therefore natural to study the theory of tethers in the simplest possible situation, namely, the classic soap-film geometry described above (Fig. 2). This model situation captures the essential features of the tether shape and formation without the experimentally important, but ultimately complicating, effects of volume and lipid conservation. Our quasianalytic approach exploits the smallness of the tether radius, and is complementary to important numerical work by various groups, most notably Heinrich *et al.* [6]. We begin our analysis in Sec. II with a discussion of shells, balloons, and soap films in order to contrast their familiar mechanical properties with the peculiar properties of lipid bilayer membranes. The latter are the subject of Sec. III, which defines precisely the model problem. Section IV reviews the elements of the soap-film problem that are relevant for understanding the formation of tethers, the subject of Sec. V. There we use asymptotic methods to solve the linearized equations for small ring displacements and large tensions, and find that the membrane shape is that of a catenoid with a small elastic boundary layer surrounding the smaller ring (the point force). At a critical ring separation, a tether forms from the elastic boundary layer. The tether shape is studied analytically and numerically, and a connection is made with the classic film-coating calculations of Landau and Levich [14], as well as Bretherton's related calculation of the shape of a long air bubble rising in a fluid-filled capillary tube [15]. Section VI is the conclusion. The Appendix reviews the subtleties that arise when comparing
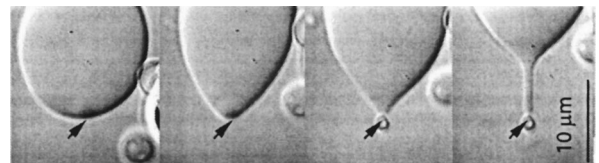

FIG. 1. Equilibrium shapes of a vesicle subject to various point forces [10]. An optical tweezer exerts the point force, which increases from left to right. Figure courtesy of D. Fygenson.

*Electronic address: Thomas_Powers@brown.edu
†Electronic address: huber@umb.edu
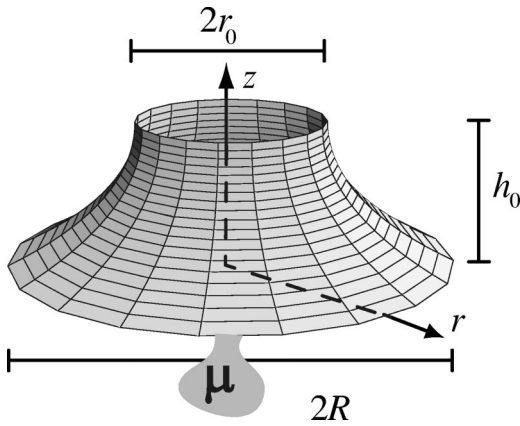‡Electronic address: gold@physics.arizona.edu

FIG. 2. Model problem. Two parallel rings with aligned centers are connected by a lipid bilayer membrane in contact with a lipid reservoir at fixed chemical potential (per unit area) μ.

the variational approach for lipid bilayer membrane elasticity to that of moment and force balance.

II. SHELLS, BALLOONS, AND SOAP FILMS

Before exploring the lipid bilayer membrane properties that give rise to tethers, we review three examples of elastic surfaces encountered at the macroscopic scale: shells, balloons, and soap films. Much intuition about elastic surfaces derives from these canonical examples. Some of this intuition can be directly applied to lipid membranes, but it is illuminating to point out the crucial differences as well.

Shells are solid surfaces with a small thickness and a preferred shape in the absence of external stresses. A plate is a shell with a flat preferred shape. It is a matter of common experience that the force required to bend a thin plate through a certain displacement is much less than that required to stretch the plate through the same displacement. The plate can undergo large displacements through bending without subjecting each element to large stress; thus, linear elasticity is valid and the nonlinearities in the equations for shape are solely geometrical. In the limit of small plate thickness, stretching energy exceeds bending energy, since bending is differential stretching. Deformations without stretching are, therefore, of lowest energy [16]. These deformations, in which the distances between nearby points remain fixed, are called *isometric*. For example, the axisymmetric isometric deformations of the plane are cylinders and cones [17]. Note that a shearing motion locally stretches the plate, even if the total area does not change. Bending energy (and possibly boundary conditions) removes the degeneracy when, as in the case of a flat plate, there is a multiplicity of isometric deformations. Bending also plays a role near boundaries and point forces. A familiar example of a plate with vanishing thickness is a sheet of paper, which bends easily but hardly stretches or shears. The reader can easily verify that a sheet of paper subject to a point force forms a cone with a single fold, a shape with twofold symmetry. For shells, the isometric constraint on deformations is even more severe. *Any* deformation of a sphere requires some local stretching or shearing: no almost-spherical shapes are isometric to the sphere. A

spherical shell is *geometrically rigid*. On the other hand, there are isometric small deformations of a spherical shell with a circular hole [16]. The problem of determining the geometric rigidity of an axisymmetric shell with boundaries was solved using the qualitative theory of differential equations [18]; for recent progress using a geometric approach, which can be generalized to nonaxisymmetric shells, see Ref. [19].

Next, consider the case of balloons. Like plates with vanishing thickness, there is virtually no cost to bend a section of a balloon compared to the cost of stretching or shearing. However, deformations are not required to be isometric since the cost of stretching is also low. Such a material is called a ''membrane'' in the theory of elasticity [16]; to avoid confusion with lipid bilayer membranes, this terminology will not be used. Since real balloons are easily stretched out of the linear elastic regime, the nonlinearity of the governing equations arises from the constitutive relations as well as the geometry of large deformations. Anyone who has inflated a cylindrical balloon has seen a phenomenon very much similar to the tethers of Fig. 1. A partially inflated balloon has two cylindrical regions, one smaller than the other, which are smoothly connected by a junction region. However, this phenomenon differs fundamentally from that of tether formation in lipid bilayer membranes for several reasons. No point force is required to make a balloon form a tether; it arises from the nonlinear constitutive relation between tension and areal extension, which is reflected by a nonmonotonic p-V curve, reminiscent of the isotherms of the van der Waals equation of state for a gas [20]. The material in the larger cylinder is stretched more, and thus has a higher tension. The smaller cylinder is under smaller tension; the difference between the axial force of each tension is precisely balanced by the net pressure on the junction region. Thus, a pressure jump across the surface of the balloon is crucial for this tether. Below it is shown that such a pressure jump is unnecessary for lipid bilayer membrane tethers.

Our final canonical example is the ''ideal'' soap film, which simply minimizes area subject to the boundary conditions and volume constraints. Effects such as thickness variations and draining do not have a clear counterpart in the case of lipid bilayer membranes, and are therefore disregarded. Since soap films are liquid, the static in-plane shear rigidity vanishes, and the notion of geometric rigidity does not apply. Deformations need not be isometric and folds are not required to bend a flat film into a hemisphere. (There can be solidlike folding behavior in liquid-film dynamics whenever bending flows are preferable to extensional flows [21].) Unlike the case of plates, interfacial tension is a material property of the soap film, and is not determined by external forces. To imagine poking a soap film with a point force, consider again the geometry of two rings described in the introduction, but now take one ring radius to be much smaller than the other. Equilibrium solutions exist only when the ring separation is less than a critical separation, comparable to the radius of the smaller ring. At a slightly larger separation, the film breaks. The equilibrium shapes are shallow catenoids, and look nothing like tethers (structures reminiscent of thin tethers form during the rupture of a soap film,

but these have a dynamical origin; see Ref. [22]). However, these shallow catenoidal shapes resemble the junction region between the tether and vesicle of Fig. 1. Soap films and catenoids will be studied in more detail in Sec. IV.

Lipid bilayer membranes have elements of each of these examples. Like macroscopic plates, lipid membranes resist bending, but they are typically fluid and therefore lack geometric rigidity, similar to soap films. The interplay between these solidlike and fluid properties leads to the formation of tethers.

III. LIPID BILAYER MEMBRANES

A. Bending elasticity

There is a vast literature on the mechanics of lipid bilayer membranes (e.g., see Ref. [23]). Here we review only the aspects relevant to tethers. Lipid molecules are amphiphilic, composed of two oily hydrophobic chains attached to a polar hydrophilic head. Lipids self-assemble in aqueous solution to shield the chains from the water, forming micron-size bilayer surfaces. In the fluid phase, a typical self-diffusion constant for a lipid molecule in a membrane is of order 10^{-8} cm^2/sec [24]. The membrane is clearly a two-dimensional fluid over the time scale of typical tether experiments: a molecule will diffuse from one side of a one-micron radius spherical vesicle to the other in about a second. Hence, there is no in-plane static shear modulus. However, membranes have a nonzero bending modulus since bending the membrane compresses and extends the slightly elastic heads and tails of the lipid molecules. The fluid nature of the membrane constrains the form of the elastic energy to depend only on the *shape* of the membrane. To lowest order in curvatures, the bending energy is given by the expression of Canham [25] and Helfrich [26],

$$\mathcal{E}_{el} = \int dS \left[\frac{\kappa}{2}(2H)^2 + \frac{\bar{\kappa}}{2}K \right], \qquad (1)$$

where H is the mean curvature of the membrane surface and K is the Gaussian curvature (κ and $\bar{\kappa}$ are elastic constants). In terms of the principal radii of curvature R_1 and R_2 at a point on the surface, $2H = 1/R_1 + 1/R_2$ and $K = 1/(R_1 R_2)$. Explicit formulas for these curvatures will be given below. For simplicity, suppose that there is no difference between the two sides of the bilayer; hence, there is no spontaneous curvature. The Gaussian curvature term is typically dropped in studies of vesicles since it amounts to the sum of a deformation-independent term and a boundary term by the Gauss-Bonnet theorem,

$$\int dS\, K + \oint ds\, \kappa_g = 2\pi\chi, \qquad (2)$$

where χ is the Euler-Poincaré characteristic and κ_g is the geodesic curvature of the boundary of the surface [17]. Note that a more detailed treatment of the formation of tethers in vesicles would require additional terms of the generalized

bilayer couple model [27–31]. In the spirit of explaining tether formation in the simplest possible context, these are disregarded.

Although typical values for the elastic bending modulus κ are $(10–15)\, k_B T$, thermal fluctuations easily excite long-wavelength bending modes since the elastic energy vanishes as the fourth power of the wave number for fluctuations about a flat sheet. These fluctuations lead to an entropic area elasticity similar to that of semiflexible polymers, as is most directly illustrated by the experiments of Evans and Rawicz [32] (see also Ref. [33]). In these experiments, the tension in a vesicle is measured as a function of apparent area by suctioning a small amount of the vesicle membrane into a pipet. At low suctions (or low tensions), the resistance to stretching is the entropic penalty of reducing the number of fluctuating modes. At high tensions, most of the thermal ripples have been smoothed out, and the resistance to stretching is mainly due to the membrane's intrinsic area elasticity. Thermal fluctuations are therefore negligible for the high tension regime considered here.

B. Model problem and nondimensionalization

As in the Introduction, consider a lipid membrane spanning two rings that are initially concentric and lying in the plane $z = 0$ (see Fig. 2). The outer ring of radius R remains in this plane, but the height h_0 of the inner ring will be varied. Measuring all lengths in units of the radius R, henceforth $R = 1$. The inner ring then has radius $r_0 \ll 1$. Later, we will take $r_0 \to 0$ to model the application of a point force. For comparison with the case of soap films and also for the numerical approach, it is convenient to keep r_0 nonzero for now. Assume that there is a reservoir of lipid at a fixed chemical potential (per unit area) μ. Further suppose this "surface tension" is very large compared to the bending elasticity, $\mu R^2 \gg \kappa$. Thermal fluctuations are therefore negligible. Since the membrane has edges, the Gaussian modulus $\bar{\kappa}$ affects the shape through the boundary conditions [recall the geodesic curvature term of Eq. (2)]. For simplicity, we disregard this effect and set $\bar{\kappa} = 0$.

Our model is closest in spirit to the tether experiments of Evans and Yeung [1] mentioned earlier. The pipet suction sets the value of the tension μ and the small amount of lipid projecting inside the pipet serves as a reservoir. In the experiments, the vesicle is under pressure and is therefore curved, whereas in our model there is no pressure jump across the initially flat membrane. The role of the pressure in vesicle tethers is small since the tether curvature is much larger than the vesicle curvature for high tension. In fact, it is shown in Sec. V B 2 that the pressure leads to a subleading correction to the tether radius.

The complete specification of the model problem requires defining the boundary conditions at the rings. The tangent plane of the surface at the point force is perpendicular to the force if the line of action is along the axis of symmetry. Since the role of the small ring is to mimic a point force, the membrane is clamped so that the tangent plane at each point on the boundary (with the small ring) is in the plane of the small ring. The ring at $r = 1$ is somewhat artificial; therefore

we choose the simplest possible boundary condition for $r = 1$, which turns out to be zero moment, $H = 0$ [16]. The outer ring acts as a hinge. Defining the dimensionless parameter

$$\epsilon \equiv \frac{\kappa}{\mu R^2}, \qquad (3)$$

(recall $R = 1$), the problem is to minimize the energy (measured in units of μR^2)

$$\mathcal{E} = \int dS + \frac{\epsilon}{2} \int dS (2H)^2 \qquad (4)$$

for given ring separation h_0 subject to the boundary conditions and $\epsilon \ll 1$. Equation (4) casts the tether problem into the same form as the classic variational problem for a minimal surface ($\epsilon = 0$).

C. Euler-Lagrange equations

The derivation of the Euler-Lagrange equations from the energy of Eq. (4) is somewhat lengthy but straightforward [34]. The result is

$$2\epsilon(\nabla^2 H + 2H^3 - 2HK) - 2H + \Delta p = 0, \qquad (5)$$

where ∇^2 is the covariant Laplacian on the surface. Δp (the Lagrange multiplier enforcing volume conservation for closed vesicles) measured in units of μ/R (in other words, μ) is zero for our soap-film geometry, but it is included in Eq. (5) for later discussion of the effect of pressure on tether shape. Note that $\epsilon = 0$ and $\Delta p = 0$ yields the minimal-surface equation, $H = 0$. Since the membrane shape is a surface of revolution, natural coordinates for the surface are φ the azimuthal angle and s arclength along a meridian. Arclength is measured from the inner ring, which has coordinate $s = 0$. The position of a point on the surface is, therefore, $\mathbf{X}(s, \varphi) = r(s)\hat{\mathbf{r}} + z(s)\hat{\mathbf{z}}$, where r and z are cylindrical coordinates. Note that $r_s^2 + z_s^2 = 1$, since s is arclength.

With these choices, the metric, or first fundamental form, is

$$g_{ij} d\xi^i d\xi^j = ds^2 + r^2 d\varphi^2, \qquad (6)$$

where $\xi^1 = s$ and $\xi^2 = \varphi$. The second fundamental form is

$$K_{ij} d\xi^i d\xi^j = (z_s r_{ss} - r_s z_{ss}) ds^2 - r z_s d\varphi^2, \qquad (7)$$

where $z_s = dz/ds$, etc. We follow the usual conventions for raising and lowering indices using the inverse g^{ij} of the metric tensor. Thus, $g^{ik} g_{kj} = \delta^i_j$, $K^i_j = g^{ik} K_{kj}$, and

$$H \equiv \frac{1}{2} g^{ij} K_{ij} = \frac{1}{2} \left[\frac{r_{ss}}{z_s} - \frac{z_s}{r} \right], \qquad (8)$$

$$K \equiv \det K^i_j = -\frac{r_{ss}}{r}, \qquad (9)$$

$$\nabla^2 \equiv \frac{1}{\sqrt{g}} \partial_i g^{ij} \sqrt{g} \partial_j = \frac{1}{r} \frac{d}{ds} r \frac{d}{ds}, \qquad (10)$$

where g is the determinant of the metric tensor g_{ij} and $r_s^2 + z_s^2 = 1$ was used to simplify (8).

The Euler-Lagrange equation (5) for an axisymmetric shape is a nonlinear ordinary differential equation, easily solved with numerical methods. However, more insight is gained by exploiting the smallness of ϵ. Since ϵ multiplies the term in Eq. (5) with the highest number of derivatives, there will be a boundary layer. The layer occurs where the boundary conditions are incompatible with Eq. (5) with $\epsilon = 0$. It is now clear why the zero moment $H = 0$ boundary condition is the most natural condition at the larger ring: this boundary condition is compatible with the minimal-surface equation and does not lead to a boundary layer at the larger ring. The clamped boundary condition at the smaller ring, however, is incompatible with the minimal-surface equation, since the ring must exert a moment on the surface to keep it clamped. In this boundary layer, bending and tension balance and the shape is determined by the full Euler-Lagrange equation, where the smallness of ϵ is offset either by large s derivatives or large curvatures. Balancing $\epsilon \nabla^2 H$ with H in Eq. (5) reveals that the boundary layer thickness scales as $\sqrt{\epsilon}$. In the outer region, beyond the elastic boundary layer, bending is unimportant and the shape is governed by the minimal-surface equation, $H = 0$. The only nonplanar axisymmetric minimal surface is a catenoid, the surface of revolution generated by a catenary [17]. Thus, the membrane forms a catenoid in the outer region. The following section reviews basic facts about catenoids.

IV. CATENOID LORE

We noted in the preceding section that setting $\epsilon = 0$ and $\Delta p = 0$ in Eq. (5) results in the minimal-surface equation $H = 0$. To leading order, the outer solution to Eq. (5) is given by exactly the same condition. The solution to the minimal-surface equation is conveniently found by applying Noether's theorem directly to the energy functional (4) with $\epsilon = 0$. To this end, rewrite dS in terms of $r(z)$,

$$\mathcal{E} = \int d\varphi \, dz \, r \sqrt{1 + r_z^2}. \qquad (11)$$

The conserved quantity associated with the invariance of the integrand of Eq. (11) with respect to translations in z is the axial force F necessary to hold the rings apart at a given separation,

$$\frac{F}{2\pi} = \frac{r}{\sqrt{1 + r_z^2}}. \qquad (12)$$

The radius r attains its minimum value $b = F/(2\pi)$ when $r_z = 0$. Integrating Eq. (12) yields the catenoid

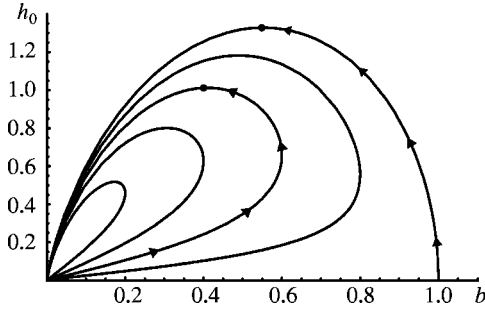$$r = b \cosh\left(\frac{z - c}{b}\right), \qquad (13)$$

FIG. 3. Ring separation h_0 vs minimum neck radius b (force by 2π) for the values $r_0=0.2,0.4,0.6,0.8$, and 1.0, proceeding from the innermost curve to the outermost curve. For a given r_0, as the rings are separated, the sequence of shapes corresponds to the trajectory marked with arrows.

where c is the z coordinate of the minimum radius. Note that b is the minimum *possible* radius; i.e., it is possibly *not* attained. The minimum radius is attained only if $c \leqslant h_0$.

The boundary condition $r(0)=1$ determines $c = \pm \cosh^{-1}(1/b)$, and thus Eq. (13) expands to

$$r = \cosh\left(\frac{z}{b}\right) \mp \sqrt{1-b^2}\sinh\left(\frac{z}{b}\right). \tag{14}$$

The upper sign is chosen as it corresponds to catenaries with a minimum neck radius at a positive value of z ($c>0$). The force F, or equivalently the minimum neck radius b, is determined by the boundary condition at the other ring: $r(h_0) = r_0$, or

$$r_0 = \cosh\left(\frac{h_0}{b}\right) - \sqrt{1-b^2}\sinh\left(\frac{h_0}{b}\right). \tag{15}$$

Solving (15) for h_0 gives the separation as a function of force

$$h_0 = b\ln\left(\frac{r_0 \pm \sqrt{r_0^2-b^2}}{1-\sqrt{1-b^2}}\right). \tag{16}$$

Note that the two branches form a closed curve in the b-h_0 plane for $r_0<1$ (Fig. 3). Since each curve has a maximum (marked with a dot for the curves $r_0=0.6$ and $r_0=1.0$), there is a critical r_0-dependent separation beyond which no catenoidal solution exists. The soap film spanning the two rings breaks just beyond this critical separation. For fixed r_0 and a given separation h_0 below the maximum, there are two catenoidal solutions. For example, Fig. 4 illustrates the two equilibrium catenoids with $r_0=1$ and $h_0=0.6$. For a given h_0, one can show that the catenoid with the larger b has less area. Thus, the solution with the smaller neck (e.g., the upper catenoid in Fig. 4) is unobservable in real soap films. In the presence of bending stiffness and a fully developed tether, it is shown below that the axial force is $2\pi\sqrt{2\epsilon}$. To see which catenoid matches onto a fully developed tether, equate the axial tether force to the axial catenoidal force $2\pi b$ to find b,
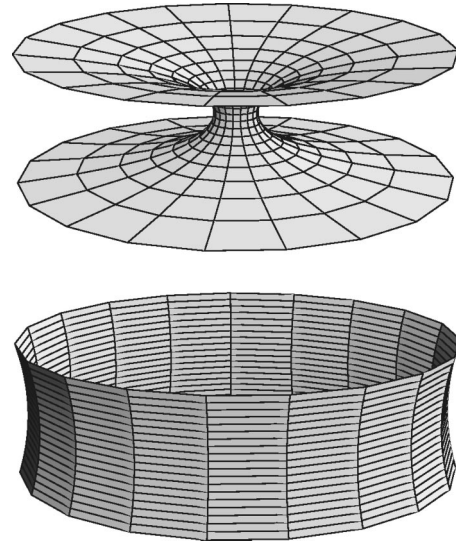

FIG. 4. The two catenoidal solutions with equal-size rings ($r_0=1$) and ring spacing $h_0=0.6$; the lower catenoid has less area.

and then use Eq. (14) to find the shape. This shape can correspond to the catenoid with greater or lesser area, depending on the value chosen for r_0.

Finally, the arrows in Fig. 3 display the trajectory of shapes as the rings are separated. The force F increases from zero to a maximum value, and then decreases slightly before the film breaks. This nonmonotonic behavior occurs in the case of tethers as well, as is shown below.

V. FROM CATENOIDS TO TETHERS

As discussed earlier, for small but nonzero ϵ, the outer region of the membrane will have a catenoidal shape, and there will be an elastic boundary layer near the small ring. This elastic boundary layer allows the attainment of the point force limit, $r_0 \to 0$, in contrast to the case of the soap film. We begin with the analysis of the case of small axial separation, $h_0 \ll 1$.

A. Small displacements

When $h_0 \ll 1$, it is most convenient to work in the Monge parameterization, in which the surface is represented by its height $z(r)$ above the plane $z=0$. To leading order in h_0, $s \approx r$, the mean curvature $H \approx (1/2)\nabla^2 z$, and the Euler-Lagrange equation reduces to

$$\epsilon\nabla^4 z - \nabla^2 z = 0, \tag{17}$$

with

$$\nabla^2 = \frac{1}{r}\frac{d}{dr}\left[r\frac{d}{dr}\right]. \tag{18}$$

The boundary conditions at the large ring $r=1$ are $z=0$ and the condition of zero moment, $\nabla^2 z=0$. At the inner ring $r=r_0$, the displacement $z=h_0$ and the slope $dh/dr=0$.

At order ϵ^0, the outer solution satisfies $\nabla^2 z_{outer}(r) = 0$, i.e.,

$$z_{outer}(r) = b_1 + b_2 \ln r. \tag{19}$$

The boundary condition on displacement at $r=1$ fixes $b_1 = 0$. The zero-moment boundary condition adds no constraint on the solution of Eq. (19); b_2 must be determined by matching to the inner solution.

Note that the outer solution diverges at the inner ring as $r_0 \to 0$; the inner solution must correct for this divergence. To find the inner solution, expand the region near $r=0$ with the rescaling $\rho = r/\sqrt{\epsilon}$. Then the inner solution satisfies

$$\frac{1}{\rho}\frac{d}{d\rho}\left(\rho\frac{d}{d\rho}\right)\left[\frac{1}{\rho}\frac{d}{d\rho}\left(\rho\frac{d}{d\rho}\right)z_{inner} + z_{inner}\right] = 0, \tag{20}$$

or

$$\frac{z_{inner}(\rho)}{h_0} = c_1 + c_2 \ln\rho + c_3 I_0(\rho) + c_4 K_0(\rho), \tag{21}$$

where $I_0(\rho)$ and $K_0(\rho)$ are modified Bessel functions. c_3 must vanish, since $I_0(\rho)$ diverges as $\rho \to \infty$ and cannot be matched to the outer solution. The boundary conditions at $r=r_0$ (i.e., $\rho=r_0/\sqrt{\epsilon}$) add two more constraints to yield

$$\frac{z_{inner}(\rho)}{h_0} = 1 + c_4\left[K_0(\rho) - K_0\left(\frac{r_0}{\sqrt{\epsilon}}\right)\right.$$
$$\left. + \frac{r_0}{\sqrt{\epsilon}}K_1\left(\frac{r_0}{\sqrt{\epsilon}}\right)\ln\left(\frac{\rho\sqrt{\epsilon}}{r_0}\right)\right]. \tag{22}$$

To match the inner and outer solutions, note that $K_0(\rho)$ decays exponentially at large ρ. Therefore, the constant terms of z_{inner} must vanish, and the coefficient of the logarithmic term of z_{inner} must match b_2. To leading order,

$$\frac{z_{outer}}{h_0} = \frac{\frac{r_0}{\sqrt{\epsilon}}K_1\left(\frac{r_0}{\sqrt{\epsilon}}\right)\ln r}{\frac{r_0}{\sqrt{\epsilon}}K_1\left(\frac{r_0}{\sqrt{\epsilon}}\right)\ln r_0 + K_0\left(\frac{r_0}{\sqrt{\epsilon}}\right)}, \tag{23}$$

and

$$\frac{z_{inner}}{h_0} = \frac{\frac{r_0}{\sqrt{\epsilon}}K_1\left(\frac{r_0}{\sqrt{\epsilon}}\right)\ln r + K_0\left(\frac{r}{\sqrt{\epsilon}}\right)}{\frac{r_0}{\sqrt{\epsilon}}K_1\left(\frac{r_0}{\sqrt{\epsilon}}\right)\ln r_0 + K_0\left(\frac{r_0}{\sqrt{\epsilon}}\right)}. \tag{24}$$

The Bessel function $K_0(r/\sqrt{\epsilon})$ cancels the logarithmic divergence of the $\ln(r)$ term of the inner solution. To construct a uniformly valid approximation $z_{composite}(r)$ for both the inner and outer regions, add the two solutions and subtract their common part [35]. This procedure yields the very compact result
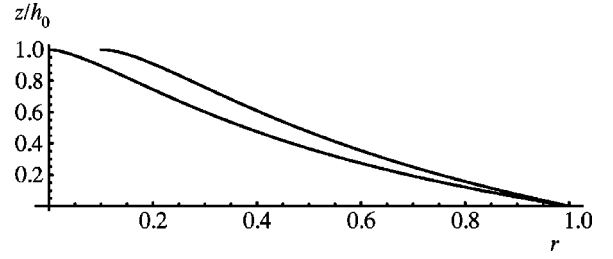

FIG. 5. Comparison of membrane profiles $z_{composite}(r)$ for $r_0 = 0.1$ (upper curve) and the point force limit $r_0 \to 0$ (lower curve).

$$z_{composite} = z_{inner}. \tag{25}$$

It is now clear why a small amount of bending elasticity allows a membrane to support a point force: the elastic boundary cuts off the divergence of the logarithm of the outer solution. To find the solutions in the limit of a point force, recall $K_1(r_0/\sqrt{\epsilon}) = \sqrt{\epsilon}/r_0 + O(r_0/\sqrt{\epsilon})$ and $K_0(r_0/\sqrt{\epsilon}) = -\gamma + \ln(2\sqrt{\epsilon}/r_0) + O[(r_0/\sqrt{\epsilon})^2]$, where $\gamma = 0.5772\ldots$ is the Euler constant. Thus

$$z_{composite}(r) = h_0 \frac{\ln r + K_0(r/\sqrt{\epsilon})}{-\gamma + \ln(2\sqrt{\epsilon})}. \tag{26}$$

Note that the boundary condition $z_{composite}(1) = 0$ is satisfied up to terms of order $\epsilon^{1/4}\exp(-1/\sqrt{\epsilon})/\ln\epsilon$ for small ϵ. Figure 5 shows that although the details of the membrane shape depend somewhat sensitively on the value of r_0, the physical limit $r_0 \to 0$ is well behaved. In this limit, the elastic boundary layer becomes a small disc of approximate radius $\sqrt{\epsilon}$ around the point force. Thus, the outer solution is roughly the catenoid that connects a ring of radius unity with a ring of radius $\sqrt{\epsilon}$. As in the preceding section, the maximum ring separation for a soap film in this situation is approximately equal to the radius of the smaller ring. Thus, as h_0 increases, the amplitude of the catenoid increases until h_0 is of order $\sqrt{\epsilon}$. Since the amplitude of the catenoid cannot increase beyond this value, the boundary layer deforms into a thin cylinder to accommodate further increases in h_0. The formation of the tether is a smooth process; there is no bifurcation.

B. Tether: Analytical approach

1. Tether radius, tether stability, and axial force

Tether formation is an intrinsically nonlinear phenomenon, and to give a complete account of the tether shape we resort to numerical methods. However, many features of the tether yield to an analytic approach. The tether radius is the most prominent such feature. Our numerical calculations will verify that the tether has a cylindrical shape between the end cap and the catenoidal junction. Thus, for our soap-film geometry with $\Delta p = 0$, the radius follows from Eq. (5) with constant mean curvature and vanishing Gaussian curvature,

$$2\epsilon H^3 - H = 0. \tag{27}$$

Since $H = -1/(2a)$ for a cylinder of radius a, the exact tether radius $a = \sqrt{\epsilon/2}$ [1]. This square-root dependence of tether radius on inverse tension has been verified experimentally by Evans and Yeung [1].

To study the stability of a tether, write $r(z) = a + u(z)$ and expand the elastic energy (4) to $O(u^2)$ [to express the metric (7) and mean curvature (8) as functions of z use $dz/ds = \sqrt{1 + r'(z)^2}$], which yields

$$\frac{\mathcal{E}}{2\pi} = \int dz \left[\left(a + \frac{\epsilon}{2a} \right) + \left(1 - \frac{\epsilon}{2a^2} \right) \left(u + \frac{au'^2}{2} \right) \right.$$
$$\left. + \frac{\epsilon a}{2} \left(u''^2 + \frac{u^2}{a^4} \right) \right]. \tag{28}$$

A total derivative term has been dropped in Ref. (28). Minimizing the u-independent terms over a yields the equilibrium tether radius. The terms linear in u vanish as expected when a takes the equilibrium value $\sqrt{\epsilon/2}$. Note that the terms quadratic in u' vanish in equilibrium as well, since the terms u and $au'^2/2$ always enter in the combination $u + au'^2/2$. This combination arises from the factor $r\sqrt{1 + r'^2}$ in the original energy. Since the remaining terms of Eq. (28) in u^2 and u''^2 are positive definite, the tether is stable. Therefore, the *equilibrium* cylinder solution does not undergo a pearling instability [36,37]. These considerations suggest that the pearling behavior induced by a rapid pull of a vesicle tether [38] arises because hydrodynamic resistance prevents the radius from instantly assuming the value appropriate to the new value of tension. This mechanism differs in detail from that of the laser-tweezer-induced instability of membrane tubes with fixed volume [37].

The tether radius determines the axial force on the catenoid. The argument hinges on the z independence of the axial force. For an undistorted cylinder with $u = 0$ and equilibrium radius $a = \sqrt{\epsilon/2}$, the total energy per unit length $\mathcal{E}/L = 2\pi\sqrt{2\epsilon}$, as easily follows from Eq. (28). Therefore, the axial force $F/(2\pi) = \sqrt{2\epsilon}$ saturates to a constant value independent of tether length once the tether has formed. Since the axial force is independent of z, the junction connecting the tether to the ring is a catenoid with $b = \sqrt{2\epsilon}$. Note that the minimum attainable radius of the limiting catenoid is twice the radius of the tether. Thus, the catenoid cannot smoothly join onto the cylindrical tether and there must be a transition region (see Fig. 6). Before analyzing this transition region in more detail, we consider the role of pressure.

2. The effects of pressure are subleading

Evans and Yeung argued that the pressure jump Δp, present in the case of a closed vesicle under tension, plays little direct role in determining the tether radius [1]. Since a sphere of radius R_0 has constant mean curvature $1/R_0$ and Gaussian curvature $1/R_0^2$, the Euler-Lagrange equation (5) in the spherical region of the vesicle reduces to the Young-Laplace law, $2H = \Delta p$ (even in the presence of bending resistance). Measuring lengths in units of R_0 (for this paragraph only), the Euler-Lagrange equation in the region of the tether becomes
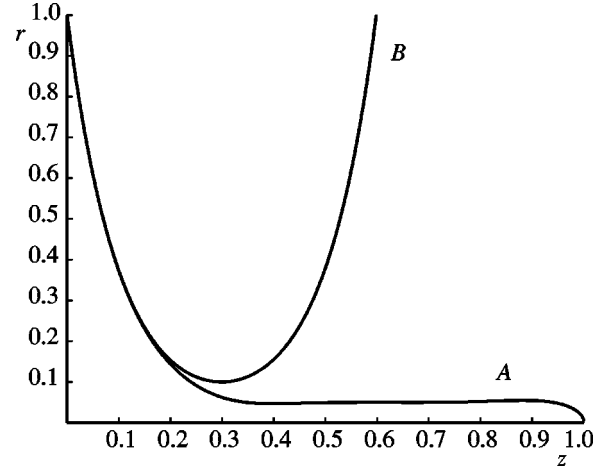

FIG. 6. Overlay of a fully developed tether (A) with radius $a = \sqrt{\epsilon/2}$ and a catenoid (B) with minimum radius $b = \sqrt{2\epsilon}$. In this example, $\epsilon = 0.005$ and the transition region lies roughly between $z = 0.2$ and $z = 0.4$.

$$\frac{\epsilon}{2a^3} - \frac{1}{a} + 2 = 0, \tag{29}$$

since the pressure jump is everywhere uniform. For small ϵ, the three solutions are

$$a = \pm \sqrt{\epsilon/2} + \epsilon/2 + O(\epsilon^{3/2}), \tag{30}$$

$$a = 1/2 - \epsilon + O(\epsilon^2). \tag{31}$$

The solution $a = -\sqrt{\epsilon/2} + O(\epsilon)$ is unphysical. The solution $a = \sqrt{\epsilon/2} + O(\epsilon)$ corresponds to the tether in the case $\Delta p = 0$. Thus, to leading order, the tether radius is unchanged and the effect of pressure appears at order ϵ. Finally, the solution with a radius near $1/2$ corresponds to a balance of pressure and tension, and is not relevant for tethers.

Returning to our model problem with $\Delta p = 0$, an apparent paradox arises. Since an axial force is required to pull the tether out of the membrane disc, there must be a tension in the membrane. This tension is isotropic, since the membrane is fluid. But consider the cylindrical portion of the tether between two fixed values of z. If this cylinder is cut in half along the long axis (Fig. 7), then each apparently experiences a resultant force due to the tension. What force balances this tension force if $\Delta p = 0$?

The paradox is most readily resolved by comparing the Euler-Lagrange equations of the variational approach with the equations that follow from force and moment balance on a membrane element, given the lipid bilayer membrane constitutive relation [1]. The Appendix recapitulates the comparison between the two approaches to the equilibrium shape equations. There it is shown that the coefficient μ of the area term in the variational energy is the tension only for minimal surfaces: $\mu = \Sigma + \epsilon H^2$, where Σ is the tension. Since the pressure jump $\Delta p = 0$, the cylindrical region of the membrane is in a state of pure bending, $\Sigma = 0$. But due to the differential stretching inherent in bending, the outer sheet is stretched and the inner sheet is compressed (Fig. 7). Since
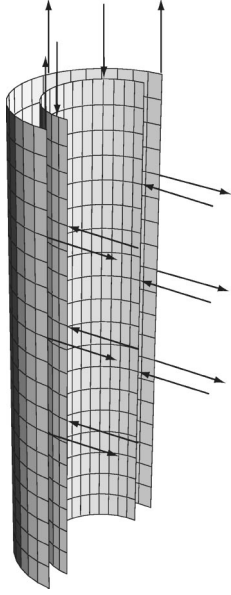
FIG. 7. Axial force due to the greater circumference of the outer leaf.

the sheets are fluid, the tension or compression in each sheet is isotropic. The compressive and tensile forces along the lines of longitude of the cylinder cancel (consistent with $\Delta p = 0$). However, since the outer sheet is longer than the inner sheet along a line of latitude, there is a net axial tension. The axial force at zero pressure jump is a manifestation of the liquid properties of lipid bilayer membranes.

3. The tether always necks twice

We have seen that the shape of a membrane subject to a point force and under high tension is best described as a boundary-layer problem, with tension dominating in the outer region and bending dominating in the inner region. This situation is reminiscent of the coating problem studied by Landau and Levich [14], and of Bretherton's bubble problem [15], in which the shapes of different regions of an interface are determined by different balances. The analogy goes further: Bretherton showed that the trailing edge of a large air bubble, rising in a capillary tube filled with viscous liquid, has a slight ripple [15]. It will now be shown that there are slight ripples in the shape of a lipid membrane at *both* ends of the cylindrical tether region. These ripples have been noticed in the numerical work of Ref. [6].

Since bending and tension are equally important in the junction region, we must rescale the variables to balance these two effects. If s_1 is the arclength corresponding to a point in the transition region, it is enough to assume that the radius $r(s_1)$ is small and close to $\sqrt{\epsilon/2}$, without any further specification of s_1. It is therefore natural to rescale the radius as in Sec. V, $r = \rho\sqrt{\epsilon}$. The further rescalings $\sigma = (s - s_1)/\sqrt{\epsilon}$ and $\zeta = [z - z(s_1)]/\sqrt{\epsilon}$ lead to a balance of the bending and tension terms,

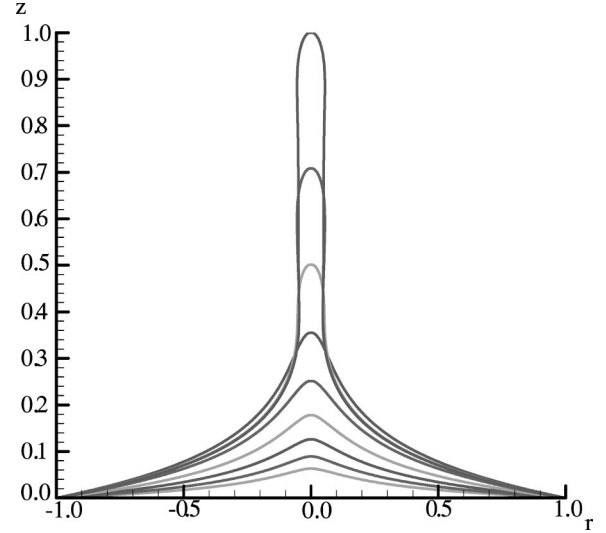$$\bar{\nabla}^2 \bar{H} + 2\bar{H}^3 - 2\bar{H}\bar{K} - \bar{H} = 0, \tag{32}$$

where

FIG. 8. Membrane shape for various ring separations; $\epsilon = 0.005$ and $r_0 = 0.005$.

$$\bar{H} = \frac{1}{2}\left[\frac{\rho_{\sigma\sigma}}{\zeta_\sigma} - \frac{\zeta_\sigma}{\rho}\right], \tag{33}$$

$$\bar{K} = -\frac{\rho_{\sigma\sigma}}{\rho}, \tag{34}$$

$$\bar{\nabla}^2 = \frac{1}{\rho}\frac{d}{d\sigma}\rho\frac{d}{d\sigma}, \tag{35}$$

and $\rho_\sigma^2 + \zeta_\sigma^2 = 1$. Therefore, the transition region is governed by the full nonlinear Euler-Lagrange equation, and there are no further simplifications arising from the smallness of ϵ. However, one can use perturbation theory to study the shape of the transition region near the tether. Let $\rho = 1/\sqrt{2} + \eta$, with $\eta \ll 1$. To leading order in η, Eq. (32) becomes

$$\eta_{\sigma\sigma\sigma\sigma} + 4\eta = 0. \tag{36}$$

Note that Eq. (36) also follows immediately from Eq. (28) with appropriate rescalings. There are four independent solutions to Eq. (36), each of the form $\eta_\alpha = C_\alpha \exp(ip\sigma)$, where $p = \pm(1 \pm i)$ and $\alpha = 1, \ldots, 4$. The shape near either end of the tether region is an exponentially damped sinusoid with wavelength $2\pi/\sqrt{\epsilon}$ and decay length $\sqrt{\epsilon}$.

C. Tether: Numerical solution

The preceding section shows that a description of the membrane shape in the junction region requires the solution of a nonlinear differential equation with no small parameters, despite the smallness of ϵ. Rather than solve this equation numerically and match the solution onto the tether and catenoidal regions, we simply solve for the complete shape numerically. Standard relaxation techniques [39] are used to solve for the shape as a function of ring displacement h_0, with a small ring of radius $r_0 = 0.005$ mimicking the point force. Figure 8 displays the membrane shape for various h_0. For small h_0, the shape is well approximated by the linear-
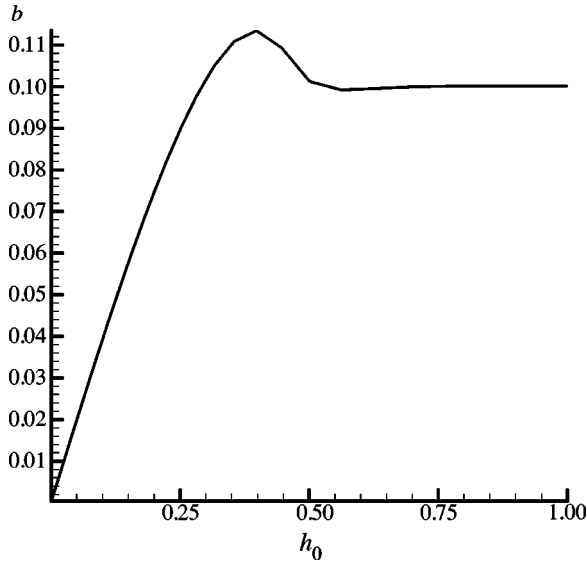
FIG. 9. Force vs displacement; $\epsilon = 0.005$, $r_0 = 0.005$.

ized catenoid with an elastic boundary layer at small radius (see Sec. V). As h_0 increases, the amplitude of the catenoid increases until the limiting catenoid with $b = \sqrt{\epsilon}$ is reached. For larger separations, a tether forms. The axial force as a function of displacement is shown in Fig. 9. Note that the force increases to a maximum and then decreases slightly before saturating to $\sqrt{2\epsilon}$. This behavior is reflected in Fig. 8, where the limiting catenoid lies inside the catenoids with slightly lower values of h_0, since these catenoids have slightly larger values of the minimum neck radius $b = F/(2\pi)$. Figure 10 shows the ripple in the junction region. The radial scale has been magnified for clarity.

VI. CONCLUSION

We have seen that tethers in our model problem are a type of boundary-layer phenomenon. In the cylindrical tether region, bending dominates, whereas tension dominates at
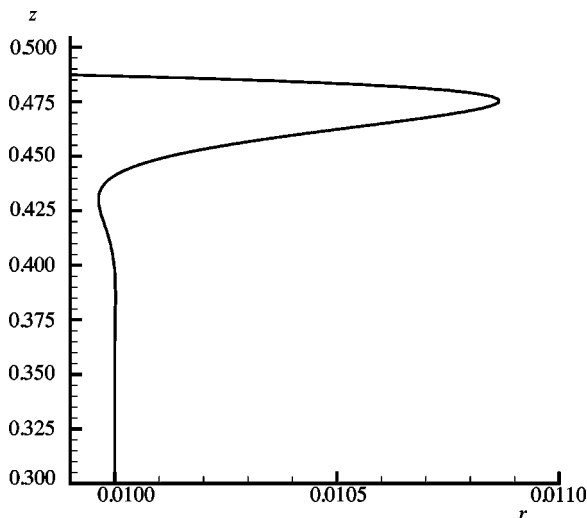

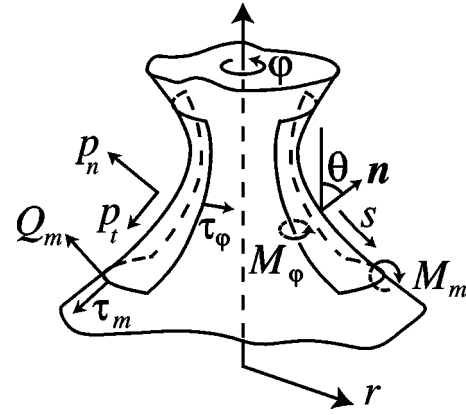FIG. 10. Ripple profile, $\epsilon = 0.0002$.

FIG. 11. Forces and moments acting on an element of an axisymmetric membrane.

larger radii. These insights carry over to the more complicated problem of tether formation in closed lipid bilayer membrane vesicles, where the quantitative details of the force vs extension will be different, since tension depends on extension. An important generalization of the problem considered here would be to study membranes with varying degrees of in-plane order, ranging from liquid crystalline to solidlike, since the liquid nature of fluid membranes is crucial for tether formation.

APPENDIX A: PLATE THEORY VS VARIATIONAL PRINCIPLE

This appendix reviews the force and moment balance relations for axisymmetric shells [1,40], and the constitutive relations for fluid membranes [1]. The approach is equivalent to the variational approach taken in the text, and elucidates the apparent paradox discussed in Sec. V B 2. Figure 11 shows the forces and moments acting on a small element of fluid membrane. Only the forces and moments that enter the shape equations are shown. τ_m is the force per unit length parallel to the meridian acting on an element edge along the azimuthal direction. τ_φ is the force per unit length in the azimuthal direction acting on an element edge along a meridian. The shearing force Q_m acts along the surface normal on an element edge along the azimuthal direction. The external stresses p_n and p_t are forces per unit area acting on the element in the normal and meridional directions, respectively. The curvature along the meridian is $c_m = d\theta/ds$, and the curvature in the azimuthal direction is $c_\varphi = \sin\theta/r$.

The balance of forces and moments is just the same as in shells. Normal stress balance requires

$$p_n = \tau_\varphi c_\varphi + \tau_m c_m - \frac{1}{r}\frac{d}{ds}(rQ_m). \tag{A1}$$

Tangential stresses balance when

$$-p_t = \frac{1}{r} \frac{d}{ds}(r\tau_m) - \frac{\tau_\varphi}{r} \frac{dr}{ds} + c_m Q_m, \qquad (A2)$$

where $dr/ds = \cos\theta$. Moment balance about the φ axis relates the shearing force Q_m to the moments per unit length M_m and M_φ,

$$Q_m = \frac{1}{r} \frac{d}{ds}(r M_m) - \frac{M_\varphi}{r} \frac{dr}{ds}. \qquad (A3)$$

It is useful to have an expression for the total axial force acting on a circle of latitude. Consider the resultant of the normal and axial stresses along the axial direction

$$r(p_n\cos\theta - p_t\sin\theta) = \frac{d}{ds}(r\tau_m\sin\theta - rQ_m\cos\theta), \qquad (A4)$$

where we have used Eqs. (A1) and (A2). In our model problem, the external stresses vanish, $p_n = p_t = 0$. Thus, $r\tau_m\sin\theta - rQ_m\cos\theta$ is a constant, the total axial force by 2π [compare with the axial force on a soap film, Eq. (12)],

$$\frac{F}{2\pi} = r\tau_m\sin\theta - rQ_m\cos\theta. \qquad (A5)$$

Returning to the derivation of the shape equations, consider now the tangential forces per unit length τ_m and τ_φ. If x denotes the coordinate across the thickness of the membrane, then

$$\tau_m = \bar{\tau} + c_\varphi M_m, \qquad (A6)$$

$$\tau_\varphi = \bar{\tau} + c_m M_\varphi, \qquad (A7)$$

where $\bar{\tau}_m = \int \tau_m dx$, $\bar{\tau}_\varphi = \int \tau_\varphi dx$, $M_m = \int x\tau_m dx$, and $M_\varphi = \int x\tau_\varphi dx$. Part of the "tension" in the membrane comes from the bending moments.

The constitutive relation for the fluid membrane completes the specification of the shape equations. Since the fluid nature implies isotropy, $\bar{\tau}_m = \bar{\tau}_\varphi$. Define the common value of tension as $\tau = \bar{\tau}_m = \bar{\tau}_\varphi$. Likewise,

$$M_m = M_\varphi = \kappa\bar{c}, \qquad (A8)$$

where $\bar{c} = c_m + c_\varphi$. Thus, the shearing force is known once the curvature of the membrane is known:

$$Q_m = \kappa \frac{d\bar{c}}{ds}. \qquad (A9)$$

Tangential force balance, Eq. (A2), becomes

$$-p_t = \frac{d}{ds}\left(\bar{\tau} + \frac{1}{2}\kappa\bar{c}^2\right). \qquad (A10)$$

In the absence of flow, the external tangential stresses vanish, and $\tau \equiv \bar{\tau} + \kappa\bar{c}^2/2$ is constant. However, $\bar{\tau}$ and $\bar{c}$ need not separately be constant.

Inserting the constitutive relations into Eq. (A1), the normal stress balance becomes

$$p_n = \tau\bar{c} - \frac{1}{2}\kappa\bar{c}(c_m - c_\varphi)^2 - \kappa\frac{1}{r}\frac{d}{ds}\left(r\frac{d\bar{c}}{ds}\right). \qquad (A11)$$

But since $\bar{c} = 2H$ and $K = c_m c_\varphi$, Eq. (A11) reduces to the Euler-Lagrange equation (5) with $\mu = \tau$.

[1] E. Evans and A. Yeung, Chem. Phys. Lipids **73**, 39 (1994).
[2] R.M. Hochmuth, N. Mohandas, and P.L. Blackshear, Jr., Biophys. J. **13**, 747 (1973).
[3] R.E. Waugh, Biophys. J. **38**, 29 (1982).
[4] R.M. Hochmuth, H.C. Wiles, E.A. Evans, and J.T. McCown, Biophys. J. **39**, 83 (1982).
[5] R.M. Hochmuth, J.-Y. Shao, J. Dai, and M.P. Sheetz, Biophys. J. **70**, 358 (1996).
[6] V. Heinrich, B. Božič, S. Svetina, and B. Žekš, Biophys. J. **76**, 2056 (1999).
[7] J. Dai and M.P. Sheetz, in *Laser Tweezers in Cell Biology*, edited by M.P. Sheetz (Academic Press, San Diego, 1998), and references therein.
[8] H. Miyamoto and H. Hotani, Adv. Biophys. **26**, 135 (1990).
[9] M. Elbaum, D.K. Fygenson, and A. Libchaber, Phys. Rev. Lett. **76**, 4078 (1996).
[10] D.K. Fygenson, J.F. Marko, and A. Libchaber, Phys. Rev. Lett. **79**, 4497 (1997).
[11] V. Emsellem, O. Cardoso, and P. Tabeling, Phys. Rev. E **58**, 4807 (1998).
[12] N. Sciaky *et al.*, J. Cell Biol. **139**, 1137 (1997).
[13] E. Evans, H. Bowman, A. Leung, D. Needham, and D. Tirrell, Science **273**, 933 (1996).
[14] L. Landau and B. Levich, Acta Physicochim. URSS **17**, 42 (1942).
[15] F.P. Bretherton, J. Fluid Mech. **10**, 166 (1961).
[16] L. Landau and E.M. Lifshitz, *Theory of Elasticity*, 3rd ed. (Pergamon Press, Oxford, 1986).
[17] D.J. Struik, *Lectures on Classical Differential Geometry*, 2nd ed. (Dover, New York, 1961).
[18] S. Cohn-Vossen, Math. Ann. **102**, 10 (1929).
[19] B. Audoly, C. R. Acad. Sci., Ser. I: Math. **328**, 313 (1999).
[20] E. Chater and J.W. Hutchinson, in *Phase Transformations and Material Instabilities in Solids*, edited by M.E. Gurtin (Academic Press, Orlando, 1984).
[21] R. da Silveira, S. Chaieb, and L. Mahadevan, Science **287**, 1468 (2000).
[22] Y.J. Chen and P.H. Steen, J. Fluid Mech. **341**, 245 (1997).
[23] U. Seifert, Adv. Phys. **46**, 13 (1997).
[24] B. Alberts, *Molecular Biology of the Cell*, 3rd ed. (Garland Publishing, New York, 1994).

[25] P. Canham, J. Theor. Biol. **26**, 61 (1970).

[26] W. Helfrich, Z. Naturforsch. C **28**, 693 (1973).

[27] W. Helfrich, Z. Naturforsch. C **29**, 510 (1974).

[28] E.A. Evans, Biophys. J. **14**, 923 (1974).

[29] E.A. Evans, Biophys. J. **3**, 265 (1980).

[30] B. Božič, S. Svetina, B. Žekš, and R.E. Waugh, Biophys. J. **61**, 963 (1992).

[31] L. Miao, U. Seifert, M. Wortis, and H.-G. Döbereiner, Phys. Rev. E **49**, 5389 (1994).

[32] E. Evans and W. Rawicz, Phys. Rev. Lett. **64**, 2094 (1990).

[33] W. Rawicz, K.C. Olbrich, T. McIntosh, D. Needham, and E. Evans, Biophys. J. **79**, 328 (2000).

[34] Z.-C. Ou-Yang and W. Helfrich, Phys. Rev. A **39**, 5280 (1989).

[35] M. Van Dyke, *Perturbation Methods in Fluid Mechanics* (The Parabolic Press, Stanford, 1975).

[36] R. Bar-Ziv and E. Moses, Phys. Rev. Lett. **73**, 1392 (1994).

[37] R.E. Goldstein, P. Nelson, T. Powers, and U. Seifert, J. Phys. II **6**, 767 (1996).

[38] R. Bar-Ziv, E. Moses, and P. Nelson, Biophys. J. **75**, 294 (1998).

[39] W.H. Press, S.A. Teukolsky, W.T. Vetterling, and B.P. Flannery, *Numerical Recipes in C*, 2nd ed. (Cambridge University Press, Cambridge, 1992).

[40] A.E.H. Love, *A Treatise on the Mathematical Theory of Elasticity*, 4th ed. (Dover, New York, 1944).